ACS OMEGA

http://pubs.acs.org/journal/acsodf

Article

Predicting Reaction Mechanisms for the Threonine-Residue Stereoinversion Catalyzed by a Dihydrogen Phosphate Ion

Tomoki Nakayoshi, Koichi Kato, Eiji Kurimoto, Yu Takano, and Akifumi Oda*

Cite This: *ACS Omega* 2022, 7, 18306−18314

Read Online

ACCESS | Metrics & More | Article Recommendations | Supporting Information

ABSTRACT: The stereoinversion of amino acid residues in proteins is considered to trigger various age-related diseases. Serine (Ser) residues are relatively prone to stereoinversion. It is assumed that threonine (Thr) residues also undergo stereoinversion, which results in the formation of the D-*allo*-Thr residue, by the same mechanisms as those for Ser-residue stereoinversion; however, D-*allo*-Thr residues have not been detected in vivo. To date, although Ser-residue stereoinversion has been suggested to progress via enolization, plausible reaction mechanisms for Thr-residue stereoinversion have not been proposed. In this study, we investigated the pathway of Thr-residue enolization and successfully identified the three types of plausible reaction pathways of Thr-residue stereoinversion catalyzed by a dihydrogen phosphate ion. The geometries of reactant complexes, transition states, and enolized product complexes were optimized using B3LYP density functional methods, and single-point calculations were performed for all optimized geometries using Møller−Plesset perturbation theory to obtain reliable energies. As a result, the calculated activation energies of Thr-residue stereoinversion were 105−106 kJ mol^{-1}, which were comparable with those of Ser-residue stereoinversion reported previously. The infrequency of Thr-residue stereoinversion may be due to other factors, such as the hydrophobicity and/or the steric hindrance of the γ-methyl group, rather than the high activation energies.

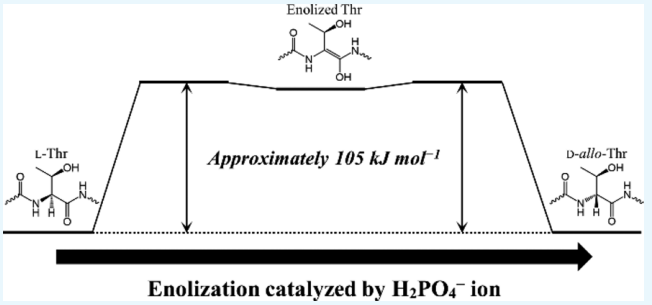

INTRODUCTION

Human proteins are composed of approximately 20 types of amino acids, which all contain asymmetric α-carbon atoms, except for glycine. Although proteins are generally considered to consist of only L-amino acids, D-amino acid residues have recently been observed in various aging tissues.[1−18] The formation of D-amino acid residues disrupts the three-dimensional structure of proteins and is considered to be relevant to age-related diseases. Only L-amino acids are used for protein biosynthesis; D-amino acid residues are considered to be post-translationally formed by the stereoinversion of L-amino acid residues. This stereoinversion occurs nonenzymatically in alkali- and/or heat-treated proteins because the α-protons of amino acid residues are slightly acidic owing to the adjacent carbonyl group.[19−23] There are many reports of the stereoinversion of aspartic acid (Asp) and serine (Ser) residues; however, there are few reports related to other proteinogenic amino acid residues.

Ser residues are relatively prone to stereoinversion in proteins, and D-Ser residues have been observed in eye lenses[9,10] and brains.[11,12] Hooi et al. demonstrated that Ser59 and Ser62 in αA-crystallin undergo stereoinversion in human eye lenses.[10] Both Ser59 and Ser62 are located in the unstructured region in αA-crystallin. In addition, the content of D-Ser residues in cataract lenses is significantly higher than that in normal human lenses. D-Ser residues are also observed in amyloid β (Aβ) in brains. Aβ contains two Ser residues, Ser8 and Ser26. The Aβ fragment containing D-Ser26 has extremely strong neurotoxicity.[12] These experimental data indicate that Ser-residue stereoinversion is associated with the pathogenesis of cataracts and Alzheimer's disease. Moreover, D-Ser residues have been detected in myelin basic proteins.[13]

Despite much research, the mechanism of Ser-residue stereoinversion was not determined for a long time. Recently, Lyons et al. proposed that Ser-residue stereoinversion proceeds by α-proton abstraction (Scheme 1).[24] The α-proton abstraction from Ser residues leads to the formation of enolized Ser residues, resulting in the disappearance of asymmetric carbons and the conversion of C_α from sp^3- to sp^2-hybridized states. The subsequent reketonization can form both L- and D-Ser residues. Theoretically, the formation of D-Ser residues can be caused by the rehydration of dehydroalanine (Dha) residues, which are dehydration products of Ser residues (Scheme 2). However, the Dha

Received: January 19, 2022
Accepted: May 18, 2022
Published: May 26, 2022

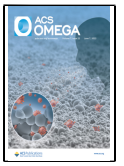

Scheme 1. Reaction Pathway for the Stereoinversion of Ser Residues via Enolized Ser Residues

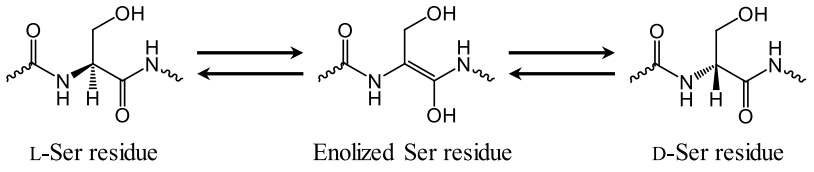

Scheme 2. Reaction Pathway for the Stereoinversion of Ser Residues via Dha Residues

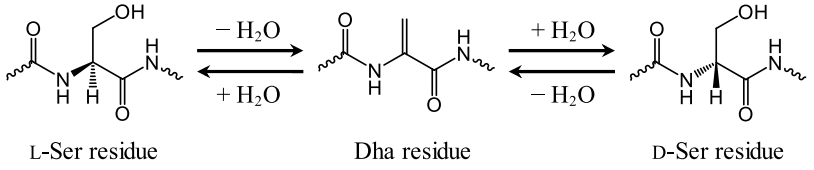

Scheme 3. Enolized Thr-Mediated Stereoinversion Pathway of Thr Residues

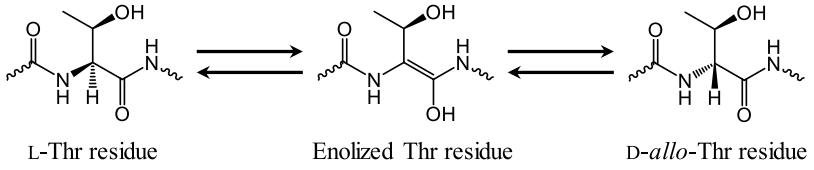

residue is hardly hydrated under physiological conditions.[24] In addition, our recent computational studies showed that the activation energies of Ser-residue dehydration and Dha-residue hydration were significantly higher than that of Ser-residue enolization.[25] These data supported that the Ser-residue stereoinversion mainly proceeds by keto-enol tautomerization. L-Ala-D/L-Glu epimerase is an enzyme that catalyzes keto-enol tautomerization with proton abstraction.[26] There are many polar amino acid residues and a coenzyme magnesium ion within the active site of L-Ala-D/L-Glu epimerase, and many hydrogen and ionic bonds are formed between the substrate peptide, enzyme, and coenzyme. These are presumed to contribute to maintaining a reactive conformation of the substrate peptide and allow for stabilization of the transition state (TS). By contrast, the Ser-residue stereoinversion is nonenzymatic, indicating that many interactions cannot be formed between the substrate and catalyst. This can explain why the Ser-residue stereoinversion proceeds slowly in vivo.

Of the proteinogenic amino acids, the chemical structure of threonine (Thr) resembles that of Ser. If the Thr-residue stereoinversion occurs via keto-enol tautomerization, D-*allo*-Thr residue is produced. To the best of our knowledge, D-*allo*-Thr residues have not yet been detected in vivo. This suggests that stereoinversion is less likely to occur in Thr residues than Ser residues. However, it is not clear why Thr-residue stereoinversion has not been observed contrary to Ser-residue stereoinversion.

To date, the detailed mechanisms for the nonenzymatic modifications of amino acid residues (including stereoinversion) have not been well elucidated. Plausible mechanisms for the nonenzymatic stereoinversion of proteinogenic Thr residues have not been proposed. Previously, quantum chemical calculations showed that the activation energies of Ser-residue stereoinversion via enol intermediates are comparable to those of typical nonenzymatic reactions.[25,27] Although Dha residues are potential intermediates of Ser-residue stereoinversion, experimental and computational evidence so far has confirmed the hypothesis that Dha residues are intermediates of stereoinversion.[24,25] Therefore, in the present study, D-*allo*-Thr residue was assumed to be obtained via enolized Thr residues (Scheme 3), as well as Ser-residue stereoinversion. In previous computational studies, it has been shown that the calculated activation energies for several nonenzymatic modifications of amino acid residues in the absence of any catalysts are too high to proceed under physiological conditions.[28−30] Therefore, some small catalytic molecules are considered to be required to progress the nonenzymatic modifications of amino acid residues. Previous computational studies showed that a dihydrogen phosphate ion ($H_2PO_4^-$) could catalyze several nonenzymatic modifications of amino acid residues.[25,27,31−40] In these studies, $H_2PO_4^-$ acts as both a Brønsted acid and base, and the catalyzed proton relays after forming appropriate complexes with amino acid residues. In the present study, to investigate why Thr-residue stereoinversion has not been observed in vivo, computational analysis was performed using quantum chemical calculations to elucidate the mechanisms for the stereoinversion of Thr residues catalyzed by $H_2PO_4^-$.

RESULTS

In the present study, a model compound of the Thr residue was used in which the Thr residue was capped with acetyl (Ace) and methylamino (Nme) groups on the *N*- and *C*-termini, respectively (Figure 1). The Ace and Nme groups are mimics of *N*- and *C*-terminal side adjacent residues, respectively. The dihedral angles φ (C−N−C_α−C) and ψ (N−C_α−C−N) characterize the main-chain conformation, and

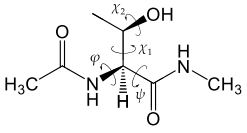

Figure 1. Chemical structure of the model compound. The dihedral angles φ and ψ characterize the main-chain conformation, and the dihedral angles χ_1 and χ_2 characterize the side-chain conformation.

https://doi.org/10.1021/acsomega.2c00372
ACS Omega 2022, 7, 18306−18314

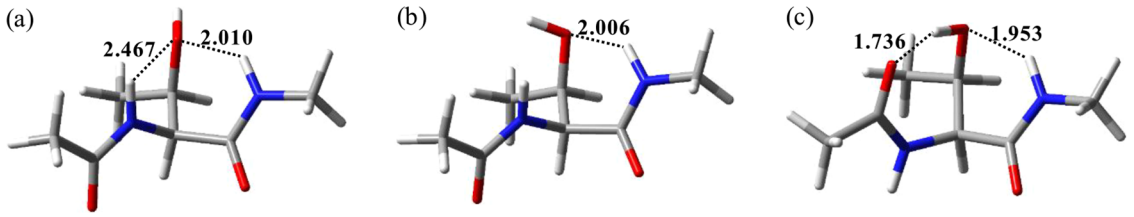

Figure 2. Optimized geometries of (a) Conformer 1 ($\varphi = -105°$, $\psi = -87°$, $\chi_1 = 55°$, and $\chi_2 = 178°$), (b) Conformer 2 ($\varphi = -117°$, $\psi = -88°$, $\chi_1 = 60°$, and $\chi_2 = -84°$), and (c) Conformer 3 ($\varphi = 77°$, $\psi = -122°$, $\chi_1 = 78°$, and $\chi_2 = -49°$). Selected interatomic distances are presented in Å. Carbon, hydrogen, nitrogen, and oxygen atoms are illustrated in gray, white, blue, and red, respectively.

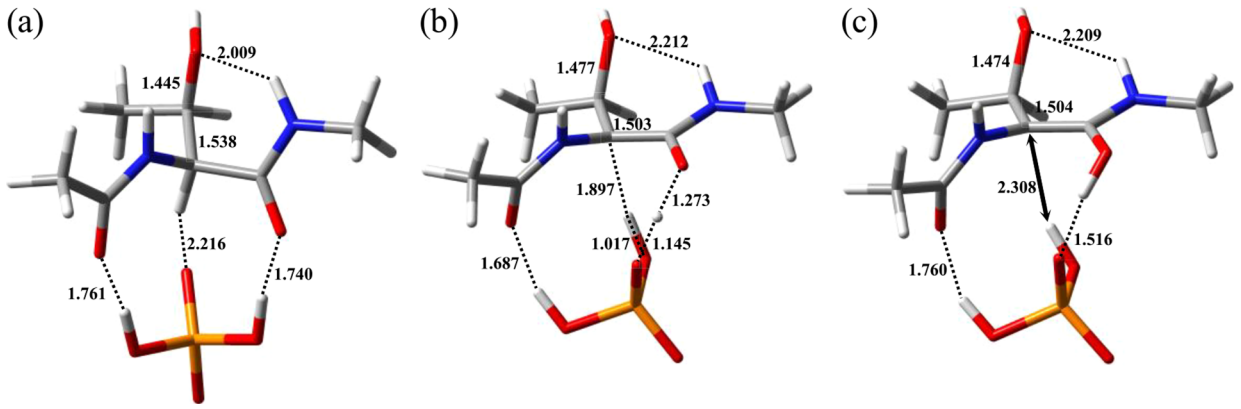

Figure 3. Optimized geometries of (a) E1-RC ($\varphi = -106°$, $\psi = -83°$, $\chi_1 = 54°$, and $\chi_2 = 177°$), (b) E1-TS ($\varphi = -127°$, $\psi = -150°$, $\chi_1 = 85°$, and $\chi_2 = 177°$), and (c) E1-EN ($\varphi = -117°$, $\psi = -159°$, $\chi_1 = 97°$, and $\chi_2 = 174°$). The single imaginary frequency of E1-TS was estimated to be 286*i* cm^{-1} (*i* means an imaginary unit). Selected interatomic distances are presented in Å. Carbon, hydrogen, nitrogen, oxygen, and phosphorus atoms are illustrated in gray, white, blue, red, and orange, respectively.

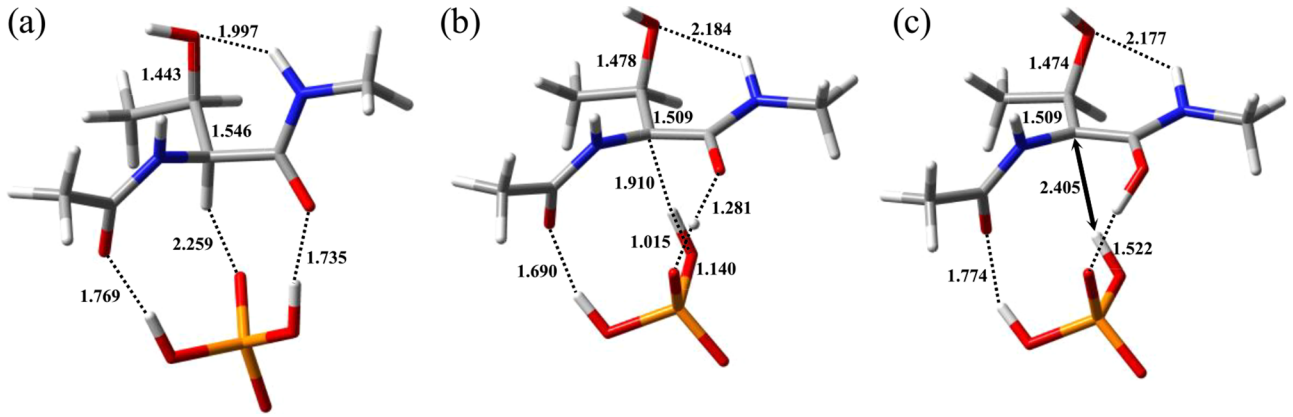

Figure 4. Optimized geometries of (a) E2-RC ($\varphi = -126°$, $\psi = -86°$, $\chi_1 = 59°$, and $\chi_2 = -82°$), (b) E2-TS ($\varphi = -126°$, $\psi = -151°$, $\chi_1 = 90°$, and $\chi_2 = -57°$), and (c) E2-EN ($\varphi = -115°$, $\psi = -161°$, $\chi_1 = 105°$, and $\chi_2 = -57°$). The single imaginary frequency of E2-TS was estimated to be 476*i* cm^{-1}. Selected interatomic distances are presented in Å. Carbon, hydrogen, nitrogen, oxygen, and phosphorus atoms are illustrated in gray, white, blue, red, and orange, respectively.

the dihedral angle χ_1 ($N-C_\alpha-C_\beta-O_\gamma$) characterizes the side-chain conformation. The calculations were performed on conformers of the model compound obtained by the conformational analysis. The conformational analysis generated 95 conformers; however, only 25 conformers with trans-configuration peptide bonds (contained in normal proteins) were generated. The reaction pathways for the Thr-residue stereoinversion could be obtained only from the three types of conformers illustrated in Figure 2, Conformers 1, 2, and 3. In these conformers, the hydrogen bond between the amide NH proton of the Nme group on the C-terminal side and the side-chain oxygen of the Thr residue was observed. The hydrogen bond lengths were 2.010, 2.006, and 1.953 Å in Conformers 1, 2, and 3, respectively. In Conformer 1, an additional hydrogen bond between the amide NH proton and the side-chain oxygen of the Thr residue was also observed (2.467 Å). The N-terminal-side main-chain conformation of Conformer 3 was significantly different from that of Conformers 1 and 2. In Conformer 3, the hydrogen bond was formed between the carbonyl oxygen of the Ace group on the N-terminal side and the side-chain OH proton (1.736 Å). This suggests that the hydrogen bonds between the side-chain hydroxyl group and the main-chain polar group greatly contribute to the stabilization of Conformers 1, 2, and 3.

The initial structures of the reactant complexes (RCs) were constructed by the placement of catalytic $H_2PO_4^-$ around each

https://doi.org/10.1021/acsomega.2c00372
ACS Omega 2022, 7, 18306−18314

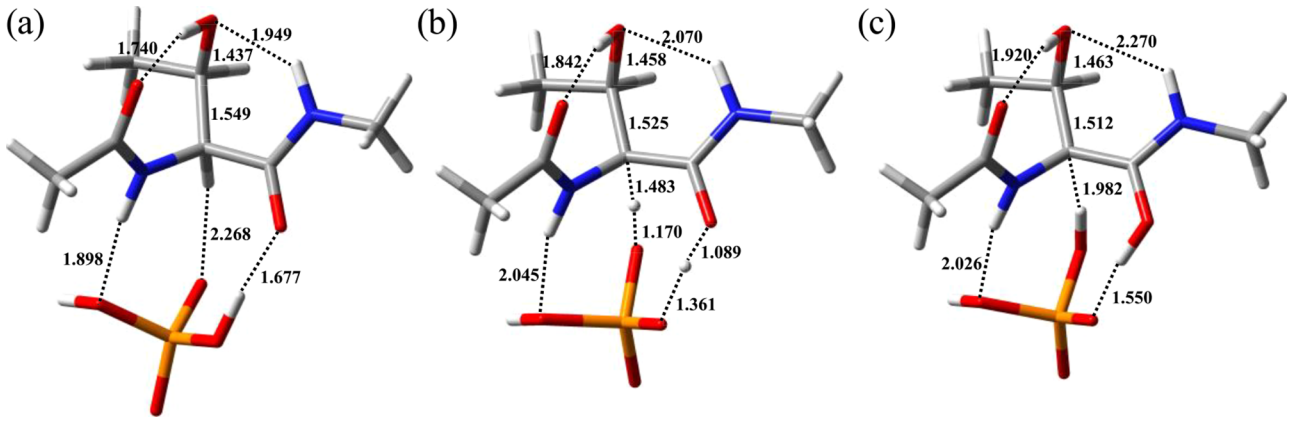

Figure 5. Optimized geometries of (a) E3-RC (φ = 73°, ψ = −124°, χ_1 = 79°, and χ_2 = −46°), (b) E3-TS (φ = 73°, ψ = −140°, χ_1 = 83°, and χ_2 = −42°), and (c) E3-EN (φ = 85°, ψ = −152°, χ_1 = 89°, and χ_2 = −41°). The single imaginary frequency of E3-TS was estimated to be 1133*i* cm^{-1}. Selected interatomic distances are presented in Å. Carbon, hydrogen, nitrogen, oxygen, and phosphorus atoms are illustrated in gray, white, blue, red, and orange, respectively.

conformer. The RCs of Conformers 1, 2, and 3 were denoted as E1-RC, E2-RC, and E3-RC, respectively. The reaction pathways of Thr-residue enolization starting from E1-RC, E2-RC, and E3-RC were defined as Pathways E1, E2, and E3, respectively. In all three pathways, the Thr residues were enolized in a single step. The TS and EN indicate the TS and the enolized intermediate complex, respectively. In addition, the optimized geometries in enolized pathways E1, E2, and E3 are named with the prefix "E1-," "E2-," and "E3-," respectively. The geometry optimizations were performed using B3LYP and the B3LYP-D3 (i.e., B3LYP with the addition of the D3 version of Grimme's dispersion) functional with the 6-31+G(d,p) basis set. In addition, for proof of internal consistencies, the geometry optimization was performed using the BHandHLYP functional with the 6-31+G(d,p) basis set. Single-point energy calculations were conducted for all the optimized geometries using the second-order Møller−Plesset perturbation theory (MP2) with the 6-311+G(d,p) basis set. Figures 3, 4, and 5 illustrate the optimized geometries in Pathways E1, E2, and E3 using the B3LYP-D3/6-31+G(d,p) level of theory, respectively. The geometries of E1-TS, E2-TS, and E3-TS optimized using the B3LYP/6-31+G(d,p) level of theory are presented in Figure S1 of the Supporting Information. There was no substantial difference in optimized geometries when using the B3LYP functional compared to the B3LYP-D3 functional. Of the three RCs (E1-RC, E2-RC, and E3-RC), the energy of E1-RC was the lowest. The relative energies calculated at the MP2/6-311+G(d,p)//B3LYP-D3/6-31+G(d,p) level of the E2-RC and E3-RC with respect to E1-RC were 3.98 and 2.77 kJ mol^{-1}, respectively. The relative energies calculated at the MP2/6-311+G(d,p)//B3LYP/6-31+G(d,p) level of the E2-RC and E3-RC with respect to E1-RC were 2.44 and 3.00 kJ mol^{-1}, respectively. Figure 6 shows the energy profiles of Pathways E1, E2, and E3. The details of the energies of the different geometries optimized using B3LYP/6-31+G(d,p) and B3LYP-D3/6-31+G(d,p) levels of theory are presented in Tables S1 and S2 of the Supporting Information, respectively.

In Pathway E1, E1-RC was converted to E1-EN via E1-TS (Figure 3). In E1-RC, two hydrogen bonds and one CH−O interaction were formed between Ace−Thr−Nme and $H_2PO_4^-$ (Figure 3a). One of the two hydrogen bonds connected the carbonyl oxygen of the Ace group with one of the OH protons

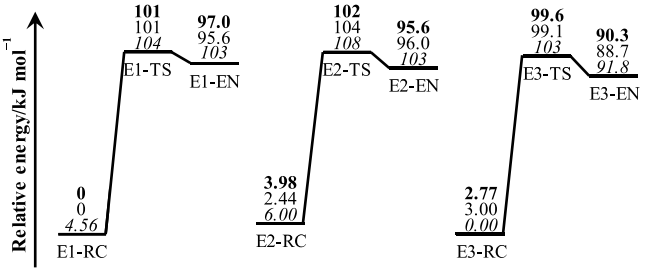

Figure 6. Energy profiles of Pathways E1−E3 for Thr-residue enolization. The relative energies with respect to E1-RC which were calculated at the MP2/6-311+G(d,p)//B3LYP-D3/6-31+G(d,p) level are shown in bold. For comparison, the relative energies calculated at MP2/6-311+G(d,p)//B3LYP/6-31+G(d,p) and MP2/6-311+G(d,p)//BHandHLYP/6-31+G(d,p) levels are shown in roman and italic, respectively.

of $H_2PO_4^-$ (1.786 Å), and another hydrogen bond connected the carbonyl oxygen of the Thr residue with the other OH proton of $H_2PO_4^-$ (1.754 Å). The CH−O interaction was formed between the α-proton of Thr and one of the oxygens in $H_2PO_4^-$ (2.394 Å). In addition, an intramolecular hydrogen bond was formed between the amide NH proton of the Nme group and the side-chain oxygen of the Thr residue (1.986 Å). When E1-TS was formed from E1-RC, the C_α−C bond length was shortened from 1.547 to 1.427 Å, and the dihedral angle was changed from −85° to −146°. These suggest that the C_α−C bond acquires a double-bond character with the α-proton abstraction. Additionally, the side-chain C_α−C_β bond was shortened from 1.541 to 1.507 Å, and the side-chain C_β−O_γ bond was elongated from 1.445 to 1.477 Å (Figure 3b). The completion of the double proton transfer mediated by $H_2PO_4^-$ resulted in E1-EN formation (Figure 3c). In E1-EN, the carbonyl oxygen of the Ace group formed two hydrogen bonds with both OH groups of $H_2PO_4^-$ (1.891 and 2.036 Å), and one oxygen of $H_2PO_4^-$ formed a hydrogen bond with the enol OH group of the enolized Thr residue (1.558 Å). Although the hydrogen-bond formation between the amide NH proton of the Nme group and the side-chain hydroxyl oxygen of the enolized Thr residue was maintained throughout Pathway E1, the distance was elongated from 1.986 to 2.210 Å. In addition, the dihedral angles ψ and χ_1 changed by 77° and 46°, respectively. The change in the dihedral angle φ was small

https://doi.org/10.1021/acsomega.2c00372
ACS Omega 2022, 7, 18306−18314

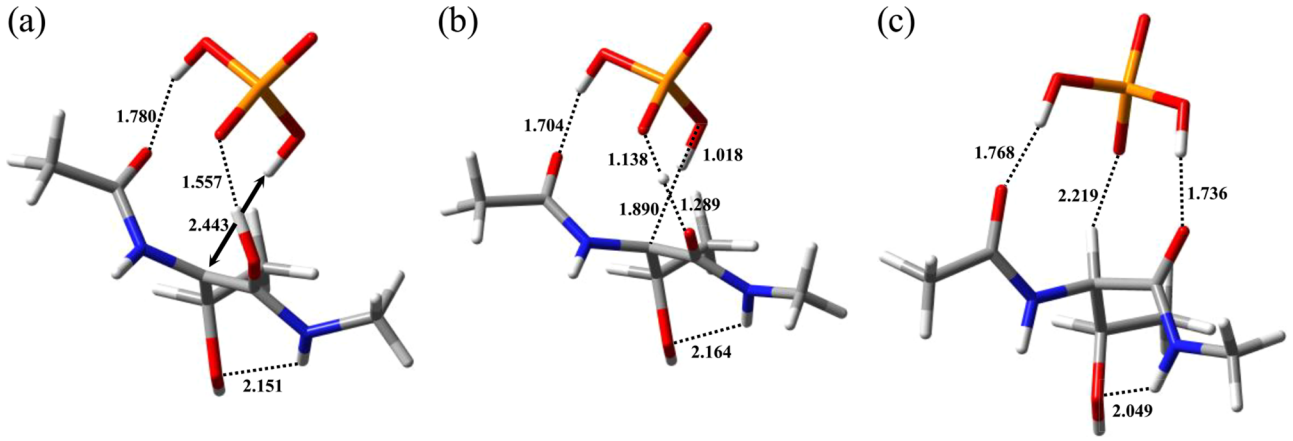

Figure 7. Optimized geometries of (a) R1-EN (φ = 120°, ψ = 159°, χ_1 = −114°, and χ_2 = −179°), (b) R1-TS (φ = 134°, ψ = 150°, χ_1 = −94°, and χ_2 = 180°), and (c) R1-PC (φ = 95°, ψ = 72°, χ_1 = −55°, and χ_2 = 178°). The single imaginary frequency of R2-TS was estimated to be 439*i* cm^{-1}. Selected interatomic distances are presented in Å. Carbon, hydrogen, nitrogen, oxygen, and phosphorus atoms are illustrated in gray, white, blue, red, and orange, respectively.

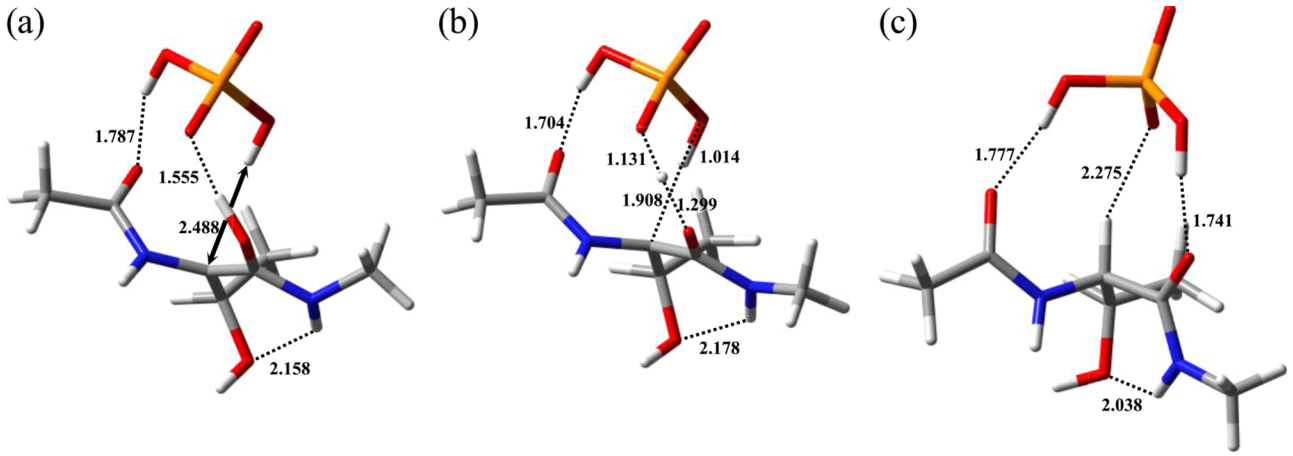

Figure 8. Optimized geometries of (a) R2-EN (φ = 118°, ψ = 160°, χ_1 = −119°, and χ_2 = 54°), (b) R2-TS (φ = 134°, ψ = 152°, χ_1 = −99°, and χ_2 = 53°), and (c) R1-PC (φ = 126°, ψ = 78°, χ_1 = −58°, and χ_2 = 82°). The single imaginary frequency of R2-TS was estimated to be 322*i* cm^{-1} (*i* means an imaginary unit). Selected interatomic distances are presented in Å. Carbon, hydrogen, nitrogen, oxygen, and phosphorus atoms are illustrated in gray, white, blue, red, and orange, respectively.

compared to the dihedral angles ψ and χ_1. The relative energies of E1-TS and E1-EN with respect to E1-RC were 101 and 93.6 kJ mol^{-1}, respectively.

In Pathway E2, E2-RC was converted to E2-EN via E2-TS (Figure 4). With the exception of the orientation of the OH bond of the side-chain hydroxyl group of the Thr residue, the geometries of E2-RC, E2-TS, and E2-EN were similar to those of E1-RC, E1-TS, and E1-EN, respectively. As shown in Figure 6, the energy of E2-RC was 2.44 kJ mol^{-1} higher than that of E1-RC. The conformational change of the main and side chains of the Thr residue in Pathway E2 was similar to that in Pathway E1. The relative energies of E2-TS and E2-EN with respect to E2-RC were 104 and 96.0 kJ mol^{-1}, respectively.

In Pathway E3, E3-RC was converted to E3-PC via E3-TS. These optimized geometries are illustrated in Figure 5. For Ser-residue enolization, a pathway similar to the Pathway E3 has already been reported.[27] The conformation of Ace−Thr−Nme and the arrangement of $H_2PO_4^-$ in E3-RC were significantly different from those in E1-RC and E2-RC (Figure 5a). In E3-RC, one hydrogen bond was formed between the OH oxygen of $H_2PO_4^-$ and the main-chain amide NH proton of the Thr residue (1.950 Å). Furthermore, as with Conformer 3, two intramolecular hydrogen bonds were formed between the side-chain hydroxyl group and the main-chain polar group of Thr residues. Two hydrogen bonds connected the Thr residue and $H_2PO_4^-$ were maintained throughout the reaction in Pathway E3. In addition, a weak interaction was observed between the C_α of the enolized Thr residue and an oxygen of $H_2PO_4^-$ (2.091 Å). During the conversion from E3-RC to E3-EN, the lengths of the two intramolecular hydrogen bonds were elongated, and the alteration was similar to those in Pathways E1 and E2. Furthermore, the dihedral angle ψ changed by 32°; however, the change in the dihedral angle χ_1 was as small as 11°. The relative energies of E3-TS and E3-EN with respect to E3-RC were 96.1 and 85.7 kJ mol^{-1}, respectively.

Thr-residue stereoinversion is completed by the reketonization of enolized Thr residues. To explore the reketonization pathways of enolized Thr residues, the conformation analyses were performed for enolized Thr residues. The conformational analyses generated 94 conformers, and 54 conformers with trans-configuration peptide bonds were obtained. Because it was difficult to perform calculations on many conformations, all conformers were optimized at the B3LYP/6-31+G(d,p)

https://doi.org/10.1021/acsomega.2c00372
ACS Omega 2022, 7, 18306−18314

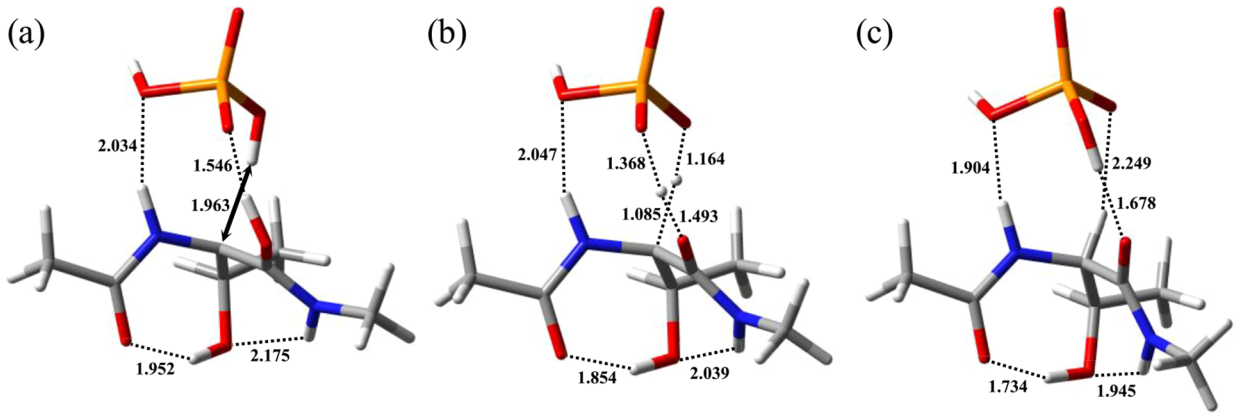

Figure 9. Optimized geometries of (a) R3-EN ($\varphi = -83°$, $\psi = 149°$, $\chi_1 = -95°$, and $\chi_2 = 46°$), (b) R3-TS ($\varphi = -73°$, $\psi = 138°$, $\chi_1 = -87°$, and $\chi_2 = 45°$), and (c) E3-EN ($\varphi = -75°$, $\psi = 119°$, $\chi_1 = -80°$, and $\chi_2 = 48°$). The single imaginary frequency of 3-TS was estimated to be 1056*i* cm^{-1}. Selected interatomic distances are presented in Å. Carbon, hydrogen, nitrogen, oxygen, and phosphorus atoms are illustrated in gray, white, blue, red, and orange, respectively.

level of theory, and those with a heavy-atom RMSD of 0.7 or less were taken as the same conformers. As a result, seven conformers were identified. For D-*allo*-Thr-residue formation, catalytic $H_2PO_4^-$ must be placed on the side opposite to where H_α was originally bound, and a proton must recombine with C_α of the enolized Thr residue on the side where the catalytic $H_2PO_4^-$ is placed. Density functional theory (DFT) calculations were performed on the complexes composed of conformers and $H_2PO_4^-$, resulting in three reaction pathways (R1, R2, and R3), which were kinetically and thermodynamically superior. In the three pathways, the enolized Thr residue is converted to the D-*allo*-Thr residue within a single step. The optimized geometries of Pathways R1, R2, and R3 are prefixed with "R1-," "R2-," and "R3-," respectively. PC indicates the product complex (consisting of the D-*allo*-Thr residue and $H_2PO_4^-$). Figures 7−9 present the optimized geometries of Pathways R1, R2, and R3 using the B3LYP-D3/6-31+G(d,p) level of theory, respectively. In addition, Figure 10 presents the

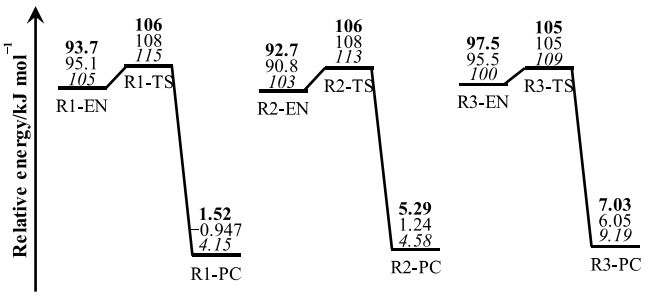

Figure 10. Energy profiles of Pathways R1−R3 for Thr-residue enolization. The relative energies with respect to E1-RC calculated at the MP2/6-311+G(d,p)//B3LYP-D3/6-31+G(d,p) level are shown in bold. For comparison, the relative energies calculated at MP2/6-311+G(d,p)//B3LYP/6-31+G(d,p) and MP2/6-311+G(d,p)//BHandHLYP/6-31+G(d,p) levels are shown in roman and italic, respectively.

energy profiles for Pathways R1, R2, and R3, respectively. The geometries of R1-TS, R2-TS, and R3-TS optimized using the B3LYP/6-31+G(d,p) level of theory are presented in Figure S2 of the Supporting Information. There was no significant difference in optimized geometries between the use of the B3LYP functional and B3LYP-D3 functional. Detailed energies of the geometries optimized using B3LYP/6-31+G(d,p) and B3LYP-D3/6-31+G(d,p) levels of theory are presented in Tables S3 and S4 of the Supporting Information, respectively. Optimized geometries of Pathways R1, R2, and R3 were similar to those of Pathways E1, E2, and E3, respectively. Note that the pathways from the Thr residue to enolized Thr residue and from enolized Thr to D-*allo*-Thr residue are not the reverse reaction as a mirror image because the β-carbon of Thr has an asymmetric center.

Additionally, all geometry optimizations were optimized using the BHandHLYP functional with the 6-31+G(d,p) basis set, and the relative energies were calculated at the MP2/6-311+G(d,p)//BHandHLYP/6-31+G(d,p) levels. As presented in Figures 6 and 10, there were no substantial differences in the activation energies calculated at all functionals.

DISCUSSION

In all the enolization pathways, the α-proton abstraction and double-bond formation in C_α−C bonds concertedly proceeded. In Pathways E1 and E2, the dihedral angles ψ and χ_1 changed significantly. In addition, although a hydrogen bond was observed between the amide nitrogen of the Nme group and the side-chain hydroxyl group, it became longer with the progression of enolization. In the enolization processes, the C_α−C bond acquires a double-bond character, and this causes the conformational change in the main chain and the weakening of the hydrogen bond between the side-chain hydroxyl oxygen and the amide NH proton of the Nme group. In contrast, in Pathway E3, although a significant change in the dihedral angle ψ was observed, that of dihedral angle χ_1 was small; the corresponding dihedral angles were 77°, 83°, and 88° in E3-RC, E3-TS, and E3-EN, respectively. This suggests that the Thr-residue enolization can proceed without major conformational changes because the two intramolecular hydrogen bonds formed between the main and side chains of Thr residues are maintained in Pathway E3. In all the enolization pathways, the dihedral angles ψ in TSs (E1-, E2, and E3-TS) ranged from −152° to −140°, which are close to the "best" values. D-*allo*-Thr residues are considered to be formed by the reketonization pathways R1, R2, and R3. Reactants of these pathways can be formed by the rotation of the Thr-residue side chain and rearrangement of catalytic $H_2PO_4^-$. As illustrated in Figures 3−5, the side-chain hydroxyl

https://doi.org/10.1021/acsomega.2c00372
ACS Omega 2022, 7, 18306−18314

Scheme 4. Contributing Structures of an Enolate-Type Thr Residue, Which Is Formed by the Abstraction of an α-Proton

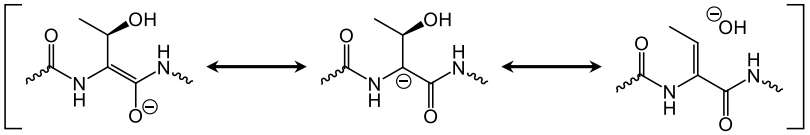

group formed hydrogen bonds with the main-chain polar group. Therefore, the rotation of single bonds in the side chain is considered to be restricted. However, the length of these intramolecular hydrogen bonds increased with the progression of the enolization. This suggested that these hydrogen bonds were weakened synchronously with the change in C_α from the sp^3- to sp^2-hybridized states upon enolization, and the restriction of the side chain is relaxed by enolization. Therefore, enolization is an important process for the acceleration of the D-*allo*-Thr-residue formation. The geometrical features observed in the optimized geometries of Pathways E1−E3 were also observed in those of Pathways R1−R3. The local activation energies of Pathways E1, E2, and E3 were calculated to be 101, 97.5, and 96.9 kJ mol^{-1}, respectively. Considering that the relative energies of E2-RC and E3-RC were 3.98 and 2.77 kJ mol^{-1} higher than that of E1-RC, the relative energies of E1-TS, E2-TS, and E3-TS with respect to E1-RC were 101, 102, and 99.6 kJ mol^{-1}, respectively. In addition, the relative energies of R1-TS, R2-TS, and R3-TS with respect to E1-RC were 106, 106, and 105 kJ mol^{-1}, respectively. Thus, there were no significant differences among energies of all the TSs. Mulliken charges of heavy atoms of the Thr-residue main chain in E-TS3 and R-TS3 were substantially different from those in other TSs, which may be due to the presence of a hydrogen bond on the main-chain amide NH proton of the Thr residue and $H_2PO_4^-$. Mulliken charges for TSs of enolization and reketonization pathways are presented in Figures S3 and S4 of the Supporting Information, respectively. On the other hand, because the activation energies and product energies did not differ significantly among pathways, the presence of a hydrogen bond in the main-chain amide NH proton of the Thr residue and $H_2PO_4^-$ is not expected to significantly affect the enolization processes.

In previous studies on Ser-residue enolization, the shortening of the side-chain $C_\alpha-C_\beta$ bond and the extension of the side-chain $C_\beta-O_\gamma$ bond were observed with the formation of TSs from the keto-form Ser residues.[25,27] These phenomena suggest that the TSs are stabilized by delocalizing the negative charge accumulating on the C_α to the antibonding orbital of the $C_\beta-O_\gamma$ bond (i.e., negative hyperconjugation).[25,27] Similar changes in the lengths of $C_\alpha-C_\beta$ and $C_\beta-O_\gamma$ bonds were observed in Thr-residue enolization and following reketonization. Furthermore, natural bond orbital (NBO) analysis was performed for all the TSs. NBO analysis showed that the antibonding orbital of the side-chain $C_\beta-O_\gamma$ bond interacts with the bonding orbital of the main-chain $C_\alpha-C$ bond in E1-, E2-, R1-, and R2-TS. Thus, the TSs are also presumed to be highly stabilized by negative hyperconjugation (Scheme 4). By contrast, the corresponding orbital interaction was not observed in E3- and R3-TS, indicating that these TSs are not as stable as those of E1-, E2-, R1-, and R2-TS. Thus, the E3- and R3-TS may not be kinetically relevant.

To the best of our knowledge, D-*allo*-Thr residues have not been found in vivo; however, the calculated activation energies of these stereoinversions were almost equal. In general, the reaction rates are affected not only by the activation energies but also by the frequency factor. The Thr residue has a methyl group at the γ-position, whereas the Ser residue does not. In all pathways E1−E3 and R1−R3, the $C_\alpha-H_\alpha$ bonds and $C_\beta-O_\gamma$ bonds were anti-periplanar, and the γ-methyl group of the Thr (or enolized Thr) residues and the catalytic $H_2PO_4^-$ were in close proximity. These steric hindrances can prevent proper access of $H_2PO_4^-$ to Thr residues. In addition, it is necessary that the site with which $H_2PO_4^-$ is bound when enolization of the Thr residues and that when reketonization of the enolized Thr residues are the opposite. Thus, the Thr residues undergoing stereoinversion need to be surrounded by solvents. However, Thr residues are more hydrophobic than Ser, which are frequently stereoinverted, and Thr residues are considered to be less frequently surrounded by solvents. It is presumed that the Thr-residue stereoinversion does not proceed rapidly owing to such factors.

CONCLUSIONS

In the present study, we successfully identified the reaction pathways for the stereoinversion of Thr residues starting from three types of RCs (E1-RC, E2-RC, and E3-RC). These RCs differed in the conformation of the Thr residue and the arrangement of the catalytic $H_2PO_4^-$. Reaction pathways of Thr-residue stereoinversion consisted of enolization and reketonization. The activation energies were slightly higher for reketonization compared to enolization; however, there were no significant differences. The calculated activation energies were approximately 105 kJ mol^{-1}. The TSs of Thr-residue stereoinversion were considered to be stabilized by negative hyperconjugation. The obtained activation energies of Thr-residue enolization were almost equal to those of Ser-residue enolization. Thus, the infrequency of Thr-residue stereoinversion in vivo is considered to be because of other factors, such as the hydrophobicity and/or the steric hindrance of the γ-methyl group. In this study, $H_2PO_4^-$ was used as a catalyst for Thr-residue stereoinversion; however, it has been shown that water, bicarbonate ions, and carboxylic acid can effectively catalyze nonenzymatic reactions of amino acid residues.[28−30,38,39,41−44] We are planning to study the potential catalytic abilities of these molecules in future studies.

METHODS

In the present study, a model compound Ace−Thr−Nme as presented in Figure 1 was used. Conformers of Ace−Thr−Nme were generated by conformational analysis. The conformational analysis was calculated using AM1 semi-empirical molecular orbital methods. The conformational analysis was conducted using Spartan software.[45,46] The conformers obtained by the conformational analysis were reoptimized by B3LYP/6-31+G(d,p) theory, and catalytic $H_2PO_4^-$ was placed around the optimized conformers.

All the energy minima and the TSs were optimized without any constraints by DFT calculations using two different methods, that is, B3LYP/6-31+G(d,p) and B3LYP-D3/6-31+G(d,p) levels of theory. For the optimized geometries, the

https://doi.org/10.1021/acsomega.2c00372
ACS Omega 2022, 7, 18306−18314

vibrational frequency calculations were performed to confirm them as energy minima (with no imaginary frequency) or TSs (with a single imaginary frequency). In addition, intrinsic reaction coordinate (IRC) calculations (followed by full geometry optimizations) were conducted to confirm that each TS was connected to two energy minima. For all calculations, the polarizable continuum model (PCM) was employed to reproduce aqueous conditions, and the dielectric constant of water in the IEF-PCM was set to 78.355 (i.e., default setting in Gaussian 16). The dielectric constant in the protein environment is often in the range of 4−10. However, as most stereoinversions of amino acid residues were so far observed at the surface of proteins exposed to water, so the dielectric constant of the solvent was set to 78.355 in this study. Moreover, for all the optimized geometries, single-point calculations were performed using the MP2/6-311+G(d,p) level of theory to obtain more reliable energies. The relative energies calculated at the MP2/6-311+G(d,p) level of theory were corrected by the zero-point energies (ZPEs) and thermodynamic corrections (to give the Gibbs energies at 1.00 atm and 298.15 K) calculated at the B3LYP/6-31+G(d,p) or B3LYP-D3/6-31+G(d,p) levels of theory. That is, all relative energies were obtained by adding the MP2 total energies, ZPEs, and Gibbs energy corrections. The computational analysis of mechanisms for the nonenzymatic reactions of amino acid residues using the MP2/6-311+G(d,p)//B3LYP/6-31+G(d,p) and MP2/6-311+G(d,p)//B3LYP-D3/6-31+G(d,p) level of theory has been performed in previous studies.[25,36] Geometry optimizations, vibrational frequency calculations, IRC calculations, and single-point calculations were performed using Gaussian 16 software.[47]

■ ASSOCIATED CONTENT

Supporting Information

The Supporting Information is available free of charge at https://pubs.acs.org/doi/10.1021/acsomega.2c00372.

Detailed energies of all optimized geometries (i.e., total energies, ZPEs, and Gibbs energies); geometries of all TSs optimized using the B3LYP/6-31+G(d,p) level of theory; Mulliken charges for all TSs (PDF)

■ AUTHOR INFORMATION

Corresponding Author

Akifumi Oda − *Faculty of Pharmacy, Meijo University, Nagoya, Aichi 468-8503, Japan; Institute of Medical, Pharmaceutical and Health Sciences, Kanazawa University, Kanazawa, Ishikawa 920-1192, Japan; Institute for Protein Research, Osaka University, Suita, Osaka 565-0871, Japan;* orcid.org/0000-0001-6487-7977; Phone: +81-52-832-1151; Email: oda@meijo-u.ac.jp

Authors

Tomoki Nakayoshi − *Graduate School of Information Sciences, Hiroshima City University, Hiroshima, Hiroshima 731-3194, Japan; Faculty of Pharmacy, Meijo University, Nagoya, Aichi 468-8503, Japan; Institute of Medical, Pharmaceutical and Health Sciences, Kanazawa University, Kanazawa, Ishikawa 920-1192, Japan*

Koichi Kato − *Faculty of Pharmacy, Meijo University, Nagoya, Aichi 468-8503, Japan; Faculty of Pharmaceutical Sciences, Shonan University of Medical Sciences, Yokohama, Kanagawa 244-0806, Japan; College of Pharmacy, Kinjo Gakuin University, Nagoya, Aichi 463-8521, Japan;* orcid.org/0000-0001-6984-2343

Eiji Kurimoto − *Faculty of Pharmacy, Meijo University, Nagoya, Aichi 468-8503, Japan*

Yu Takano − *Graduate School of Information Sciences, Hiroshima City University, Hiroshima, Hiroshima 731-3194, Japan; Institute for Protein Research, Osaka University, Suita, Osaka 565-0871, Japan;* orcid.org/0000-0002-4165-8672

Complete contact information is available at: https://pubs.acs.org/10.1021/acsomega.2c00372

Notes

The authors declare no competing financial interest.

■ ACKNOWLEDGMENTS

This work was supported by grants-in-aid for scientific research [15H01064], [17K08257], [19J23595], [19K06589], and [21K15244] from the Japan Society for the Promotion of Science. We are grateful to the Ministry of Education, Culture, Sports, Science, and Technology (MEXT) of Japan for a Grant-in-Aid for Scientific Research on Transformative Research Area (A) "Hyper-Ordered Structures Science" [20H05883]. The authors acknowledge Prof. Ohgi Takahashi for performing the conformational analysis at the manuscript revision.

■ REFERENCES

(1) Fujii, N. D-amino acids in living higher organisms. *Origins Life Evol. Biospheres* **2002**, *32*, 103−127.

(2) Ritz-Timme, S.; Collins, M. J. Racemization of aspartic acid in human proteins. *Ageing Res. Rev.* **2002**, *1*, 43−59.

(3) Fujii, N.; Saito, T. Homochirality and life. *Chem. Rec.* **2004**, *4*, 267−278.

(4) Motoie, R.; Fujii, N.; Tsunoda, S.; Nagata, K.; Shimo-oka, T.; Kinouchi, T.; Fujii, N.; Saito, T.; Ono, K. Localization of D-β-aspartic acid residue-containing proteins in various tissues. *Int. J. Mol. Sci.* **2009**, *10*, 1999−2009.

(5) Fujii, N.; Takata, T.; Fujii, N.; Aki, K.; Sakaue, H. D-amino acids in protein: The mirror of life as a molecular index of aging. *Biochim. Biophys. Acta, Proteins Proteomics* **2018**, *1866*, 840−847.

(6) Fujii, N.; Satoh, K.; Harada, K.; Ishibashi, Y. Simultaneous stereoinversion and isomerization at specific aspartic acid residues in αA-crystallin from human lens. *J. Biochem.* **1994**, *116*, 663−669.

(7) Kaji, Y.; Oshika, T.; Takazawa, Y.; Fukayama, M.; Takata, T.; Fujii, N. Localization of D-β-aspartic acid-containing proteins in human eyes. *Invest. Ophthalmol. Visual Sci.* **2007**, *48*, 3923−3927.

(8) Kaji, Y.; Oshika, T.; Takazawa, Y.; Fukayama, M.; Fujii, N. Accumulation of D-β-aspartic acid-containing proteins in age-related ocular diseases. *Chem. Biodiversity* **2010**, *7*, 1364−1370.

(9) Hooi, M. Y. S.; Truscott, R. J. W. Racemisation and human cataract. D-Ser, D-Asp/Asn and D-Thr are higher in the lifelong proteins of cataract lenses than in age-matched normal lenses. *Age* **2011**, *33*, 131−141.

(10) Hooi, M. Y. S.; Raftery, M. J.; Truscott, R. J. W. Age-dependent racemization of serine residue in a human chaperone protein. *Protein Sci.* **2013**, *22*, 93−100.

(11) Shapira, R.; Austin, G. E.; Mirra, S. S. Neuritic plaque amyloid in Alzheimer's disease is highly racemized. *J. Neurochem.* **1988**, *50*, 69−74.

(12) Kubo, T.; Nishimura, S.; Kumagae, Y.; Kaneko, I. In vivo conversion of racemized β-amyloid ([D-Ser^{26}]Aβ1−40) to truncated and toxic fragments ([D-Ser^{26}]Aβ25−35/40) and fragment presence in the brains of Alzheimer's patients. *J. Neurosci.* **2002**, *70*, 474−483.

(13) Shapira, R.; Chou, C. H. J. Differential racemization of aspartate and serine in human myelin basic protein. *Biochem. Biophys. Res. Commun.* **1987**, *146*, 1342−1349.
(14) Powell, J. T.; Vine, N.; Crossman, M. On the accumulation of D-aspartate in elastin and other proteins of the ageing aorta. *Atherosclerosis* **1992**, *97*, 201−208.
(15) Ritz-Timme, S.; Laumeier, I.; Collins, M. J. Aspartic acid racemization: Evidence for marked longevity of elastin in human skin. *Br. J. Dermatol.* **2003**, *149*, 951−959.
(16) Ritz-Timme, S.; Laumeier, I.; Collins, M. Age estimation based on aspartic acid racemization in elastin from the yellow ligaments. *Int. J. Leg. Med.* **2003**, *117*, 96−101.
(17) Ohtani, S.; Ito, R.; Arany, S.; Yamamoto, T. Racemization in enamel among different types of teeth from the same individual. *Int. J. Leg. Med.* **2005**, *119*, 66−69.
(18) Arany, S.; Ohtani, S. Age estimation by racemization method in teeth: Applications of aspartic acid, glutamate, and alanine. *J. Forensic Sci.* **2010**, *55*, 701−705.
(19) Hayase, F.; Kato, H.; Fujimaki, M. Racemization of amino acid residues in proteins and poly(L-amino acids) during roasting. *J. Agric. Food Chem.* **1975**, *23*, 491−494.
(20) Masters, P. M.; Friedman, M. Amino acid racemization in alkali treated foods proteins chemistry, toxicology, and nutritional consequences. In *ACS Symp. Ser.*; Whitaker, J. R., Fujimaki, M., Eds.; American Chemical Society: Washington, DC, USA, 1980; pp 165−194.
(21) Liardon, R.; Hurrell, R. F. Amino acid racemization in heated and alkali-treated proteins. *J. Agric. Food Chem.* **1983**, *31*, 432−437.
(22) Friedman, M.; Liardon, R. Racemization kinetics of amino acid residues in alkali-treated soybean protein. *J. Agric. Food Chem.* **1985**, *33*, 666−672.
(23) Genchi, G. An overview on D-amino acids. *Amino Acids* **2017**, *49*, 1521−1533.
(24) Lyons, B.; Jamie, J. F.; Truscott, R. J. W. Separate mechanisms for age-related truncation and racemisation of peptide-bound serine. *Amino Acids* **2014**, *46*, 199−207.
(25) Nakayoshi, T.; Kato, K.; Kurimoto, E.; Oda, A. Possible mechanisms of nonenzymatic formation of dehydroalanine residue catalyzed by dihydrogen phosphate ion. *J. Phys. Chem. B* **2019**, *123*, 3147−3155.
(26) Klenchin, V. A.; Schmidt, D. M.; Gerlt, J. A.; Rayment, I. Evolution of enzymatic activities in the enolase superfamily: Structure of a substrate-liganded complex of the L-Ala-D/L-Glu Epimerase from *Bacillus subtilis*. *Biochemistry* **2004**, *43*, 10370−10378.
(27) Takahashi, O.; Kirikoshi, R.; Manabe, N. Racemization of serine residues catalyzed by dihydrogen phosphate ion: A computational study. *Catalysts* **2017**, *7*, 363.
(28) Catak, S.; Monard, G.; Aviyente, V.; Ruiz-López, M. F. Deamidation of asparagine residues: Direct hydrolysis versus succinimide-mediated deamidation mechanisms. *J. Phys. Chem. A* **2009**, *113*, 1111−1120.
(29) Fukuyoshi, S.; Nakayoshi, T.; Takahashi, O.; Oda, A. Theoretical study on keto−enol tautomerisation of glutarimide for exploration of the isomerisation reaction pathway of glutamic acid in proteins using density functional theory. *Mol. Phys.* **2017**, *115*, 560−565.
(30) Nakayoshi, T.; Kato, K.; Kurimoto, E.; Oda, A. Computational studies on nonenzymatic pyroglutamylation mechanism of N-terminal glutamic acid residues in aqueous conditions. *Mol. Phys.* **2020**, *118*, No. e1702727.
(31) Takahashi, O.; Kirikoshi, R.; Manabe, N. Racemization of the succinimide intermediate formed in proteins and peptides: A computational study of the mechanism catalyzed by dihydrogen phosphate ion. *Int. J. Mol. Sci.* **2016**, *17*, 1698.
(32) Kirikoshi, R.; Manabe, N.; Takahashi, O. Succinimide formation from an NGR-containing cyclic peptide: Computational evidence for catalytic roles of phosphate buffer and the arginine side chain. *Int. J. Mol. Sci.* **2017**, *18*, 429.
(33) Kirikoshi, R.; Manabe, N.; Takahashi, O. Phosphate-catalyzed succinimide formation from Asp residues: A computational study of the mechanism. *Int. J. Mol. Sci.* **2018**, *19*, 637.
(34) Nakayoshi, T.; Kato, K.; Fukuyoshi, S.; Takahashi, O.; Kurimoto, E.; Oda, A. Comparison of the activation energy barrier for succinimide formation from α- and β-aspartic acid residues obtained from density functional theory calculations. *Biochim. Biophys. Acta, Proteins Proteomics* **2018**, *1866*, 759−766.
(35) Kirikoshi, R.; Manabe, N.; Takahashi, O. Phosphate-catalyzed succinimide formation from an NGR-containing cyclic peptide: A novel mechanism for deammoniation of the tetrahedral intermediate. *Molecules* **2018**, *23*, 2217.
(36) Kato, K.; Nakayoshi, T.; Kurimoto, E.; Oda, A. Computational studies on the nonenzymatic deamidation mechanisms of glutamine residues. *ACS Omega* **2019**, *4*, 3508−3513.
(37) Nakayoshi, T.; Kato, K.; Kurimoto, E.; Oda, A. Computational studies on the mechanisms of nonenzymatic intramolecular cyclization of the glutamine residues located at N-termini catalyzed by inorganic phosphate species. *ACS Omega* **2020**, *5*, 9162−9170.
(38) Kato, K.; Nakayoshi, T.; Kurimoto, E.; Oda, A. Mechanisms of deamidation of asparagine residues and effects of main-chain conformation on activation energy. *Int. J. Mol. Sci.* **2020**, *21*, 7035.
(39) Kato, K.; Nakayoshi, T.; Ishikawa, Y.; Kurimoto, E.; Oda, A. Computational analysis of the mechanism of nonenzymatic peptide bond cleavage at the C-terminal side of an asparagine residue. *ACS Omega* **2021**, *6*, 30078−30084.
(40) Asai, H.; Kato, K.; Nakayoshi, T.; Ishikawa, Y.; Kurimoto, E.; Oda, A.; Fukuishi, N. Nonenzymatic deamidation mechanism on a glutamine residue with a C-terminal adjacent glycine residue: A computational mechanistic study. *AppliedChem* **2021**, *1*, 142−155.
(41) Takahashi, O. Two-water-assisted racemization of the succinimide intermediate formed in proteins. A computational model study. *Health* **2013**, *5*, 2018−2021.
(42) Takahashi, O.; Kirikoshi, R.; Manabe, N. Roles of intramolecular and intermolecular hydrogen bonding in a three-water-assisted mechanism of succinimide formation from aspartic acid residues. *Molecules* **2014**, *19*, 11440−11452.
(43) Takahashi, O.; Kirikoshi, R.; Manabe, N. Acetic acid can catalyze succinimide formation from aspartic acid residues by a concerted bond reorganization mechanism: a computational study. *Int. J. Mol. Sci.* **2015**, *16*, 1613−1626.
(44) Nakayoshi, T.; Kato, K.; Fukuyoshi, S.; Takahashi, O.; Kurimoto, E.; Oda, A. Molecular mechanisms of succinimide formation from aspartic acid residues catalyzed by two water molecules in the aqueous phase. *Int. J. Mol. Sci.* **2021**, *22*, 509.
(45) *Spartan'14*; Wavefunction Inc.: Irvine, CA.
(46) *Spartan'16*; Wavefunction Inc.: Irvine, CA.
(47) Frisch, M.J.; Trucks, G.W.; Schlegel, H.B.; Scuseria, G.E.; Robb, M.A.; Cheeseman, J.R.; Scalmani, G.; Barone, V.; Petersson, G.A.; Nakatsuji, H.; Li, X.; Caricato, M.; Marenich, A.V.; Bloino, J.; Janesko, B.G.; Gomperts, R.; Mennucci, B.; Hratchian, H.P.; Ortiz, J.V.; Izmaylov, A.F.; Sonnenberg, J.L.; Williams-Young, D.; Ding, F.; Lipparini, F.; Egidi, F.; Goings, J.; Peng, B.; Petrone, A.; Henderson, T.; Ranasinghe, D.; Zakrzewski, V.G.; Gao, J.; Rega, N.; Zheng, G.; Liang, W.; Hada, M.; Ehara, M.; Toyota, K.; Fukuda, R.; Hasegawa, J.; Ishida, M.; Nakajima, T.; Honda, Y.; Kitao, O.; Nakai, H.; Vreven, T.; Throssell, K.; Montgomery, Jr., J.A.; Peralta, J.E.; Ogliaro, F.; Bearpark, M.J.; Heyd, J.J.; Brothers, E.N.; Kudin, K.N.; Staroverov, V.N.; Keith, T.A.; Kobayashi, R.; Normand, J.; Raghavachari, K.; Rendell, A.P.; Burant, J.C.; Iyengar, S.S.; Tomasi, J.; Cossi, M.; Millam, J.M.; Klene, M.; Adamo, C.; Cammi, R.; Ochterski, J.W.; Martin, R.L.; Morokuma, K.; Farkas, O.; Foresman, J.B.; Fox, D.J. *Gaussian 16; Rev. A.03*; Gaussian Inc.: Wallingford CT, 2016.

https://doi.org/10.1021/acsomega.2c00372
ACS Omega 2022, 7, 18306−18314